Solid-state absorption and luminescence spectroscopy of nitronyl nitroxide radicals†

Rémi Beaulac,[a] Guillaume Bussière,[a] Christian Reber,*[a] Christophe Lescop‡[b] and Dominique Luneau*[b]§

[a] *Département de Chimie, Université de Montréal, Montréal, Québec H3C3J7, Canada*
[b] *Laboratoire de Chimie Inorganique et Biologique (UMR 5046), DRFMC, CEA-Grenoble, 17 rue des Martyrs, 38054, Grenoble cedex 09, France*

Received (in New Haven, CT, USA) 5th February 2003, Accepted 1st April 2003
First published as an Advance Article on the web 26th June 2003

Low-temperature absorption and luminescence spectra of three crystalline nitronyl nitroxides are presented. For 2-(2-pyridyl)-4,4,5,5-tetramethylimidazoline-1-oxyl 3-oxide and 2-(2-benzimidazolyl)-4,4,5,5-tetramethylimidazoline-1-oxyl 3-oxide, luminescence with resolved vibronic structure is observed between 700 nm and 1100 nm. The modes forming the resolved structure have frequencies of approximately 600 cm^{-1} and 1400 cm^{-1}. They are characterized by Raman spectroscopy and electronic structure calculations. The intensity distribution within the vibronic progressions indicates small structural changes between the ground and emitting states. The lowest-energy absorption bands observed between 450 nm and 700 nm of the two luminescent compounds and of 2-cyano-4,4,5,5-tetramethylimidazoline-1-oxyl 3-oxide also show resolved structure, but the overall width of these absorption band systems is larger by a factor of 2 than that of the luminescence spectra. This difference is rationalized in terms of overlapping electronic transitions to at least two excited states arising from the $(SOMO - 1)^1(SOMO)^2$ and $(SOMO)^0(SOMO + 1)^1$ electron configurations, supported by transition energies and oscillator strengths from density functional calculations.

Introduction

An important current research direction in the area of molecular magnets is the development of multifunctional materials using a combination of magnetic and other physical properties.[1,2] Among such materials, those with novel magneto-optical properties receive particular attention in view of their potential applications in optoelectronic devices.[3] Quantitative information on the optical spectroscopy and the properties of excited electronic states is essential in the search for such materials. A recent review[4] on molecular solids incorporating free radicals indicates that their electronic spectroscopy has not been investigated in detail, in marked contrast to transition metal compounds with diamagnetic ligands, for which the effects of magnetic exchange interactions on absorption and luminescence spectra have been studied extensively.[5–7] This is surprising, as stable nitronyl nitroxide free radicals receive considerable use today as spin carriers in the field of molecular based magnets,[8] either as tectons of pure organic materials[9–13] or in combination with metal ions in the engineering of organic–inorganic materials.[14–19] Molecular solids based on radicals are highly promising systems with novel magneto-optical properties, as demonstrated recently by Matsuda and Irie.[20] By incorporating two nitronyl nitroxide moieties into a photosensitive diarylethene core, they succeeded in reversibly switching the intramolecular (radical–radical) magnetic interaction upon illumination.[20] Nitronyl nitroxides also show interesting nonlinear optical properties due to their large negative second hyperpolarizability.[21]

Room-temperature absorption spectra of nitroxides and their complexes in solution have been reported as short descriptions given when the compounds were first synthesized.[22–24] A complete study of the absorption and Raman spectra of a series of nitronyl nitroxide complexes of Cr(III) and Ni(II) was recently carried out by Kaizaki *et al.*[25,26] The authors were able to correlate the strength of the Ni(II)–radical magnetic exchange coupling with the absorption intensity.[26] A limited number of other transition metal and lanthanide complexes with nitroxide radicals have also been characterized by room temperature Raman and absorption spectroscopy.[27–29]

We recently initiated the magnetic and spectroscopic studies of a series of nitronyl nitroxides with lanthanide ions and have reported their unprecedented near-infrared luminescence centered on the radical ligand.[30,31] This has led us to investigate the low-temperature, solid-state electronic spectroscopy of uncoordinated nitronyl nitroxides, in order to characterize their excited states in the visible and near-infrared spectral regions based on the following comparison of the first full luminescence spectra and detailed absorption spectra of three different crystalline nitronyl nitroxide free radicals.

Experimental

Syntheses

2-(2-Pyridyl)-4,4,5,5-tetramethylimidazoline-1-oxyl 3-oxide (abbreviated in the following as NITPy), 2-(2-benzimidazo-

† Electronic supplementary information (ESI) available: solution absorption and luminescence spectra of NITBzImH, Raman spectra of NITBzImH and NITCN, SOMO − 2 and SOMO − 3 calculated molecular orbitals for NITCN, SOMO + 1, SOMO and SOMO − 1 calculated molecular orbitals for NITPy and output files for all PM3 and DFT calculations. See http://www.rsc.org/suppdata/nj/b3/b301479g/

‡ Present address: Organométalliques et Catalyse: Chimie et Electrochimie Moléculaires, UMR 6509, Institut de Chimie de Rennes, CNRS - Université de Rennes 1, Campus de Beaulieu, 35042 Rennes cedex, France.

§ Present address: Université Claude Bernard Lyon 1 - Bât. 305 - 43 avenue du 11 novembre 1918 – 69622 Villeurbanne cedex.

lyl)-4,4,5,5-tetramethylimidazoline-1-oxyl 3-oxide (abbreviated in the following as NITBzImH) and 2-cyano-4,4,5,5-tetramethylimidazoline-1-oxyl 3-oxide (abbreviated in the following as NITCN) were prepared according to literature methods and characterized as described earlier.[13,18,22] The molecular structures of all three compounds are shown schematically in Fig. 1.

Spectroscopic instrumentation

Absorption spectra were measured on a Varian Cary 5E spectrometer using the photomultiplier tube detector for the visible range. The sample crystals were cooled in a He gas flow cryostat (Oxford Instruments CF-1204) and the temperature was monitored with a RhFe resistor connected to an electronic controller (Oxford Instruments ITC4) to stabilize the temperature to better than ± 1 K by adjusting both a heater for the He gas cooling the sample and the gas flow valve from the He storage Dewar to the cryostat. All spectra presented in the following are unpolarized, as no strong dichroic effects were observed in preliminary spectra polarized along the optical extinction directions of simple crystals.

Luminescence was excited with the 514.5 nm and 488 nm lines of an Ar^+ ion laser. The sample crystals were again placed in the He gas flow cryostat. The emitted light was dispersed with a Spex 500M monochromator and detected with a Ge diode (Applied Detector Corporation ADC403L). This detector is sensitive in the 600 nm to 1800 nm wavelength range and its sensitivity varies very little over the range examined for the title compounds. The signal was averaged and stored with a lock-in amplifier, as described previously.[32] Raman spectra were measured using a commercial micro-Raman spectrometer (Renishaw System 3000), again with the 488.0 nm and 514.5 nm Ar^+ excitation lines. Care was taken to reduce the laser power to avoid decomposition of the compounds. This instrument was also used as a sensitive alternative to measure luminescence spectra at wavelengths shorter than 1000 nm[33] using a liquid helium flow cryostat designed for this microscope (Janis Research Supertran ST-500). The origin regions of the luminescence spectra of several lanthanide complexes with nitronyl nitroxide radical ligands were measured with this instrument, as reported in a preliminary communication.[30]

Spectroscopic results

The lowest-energy electronic transitions are characterized by the combination of luminescence and absorption spectra. Fig. 2 compares spectra for two different nitronyl nitroxide free radicals, NITPy in Fig. 2a and NITBzImH in Fig. 2b. The luminescence spectra have their onsets at very similar energies of approximately 14 820 cm^{-1} and 15 290 cm^{-1} and overall band widths at half height of approximately 1100 cm^{-1} and 2100 cm^{-1} for NITBzImH and NITPy, respectively.

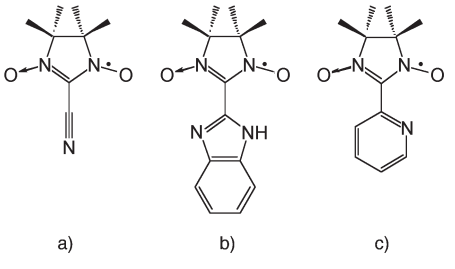

Fig. 1 Schematic representations of the nitronyl nitroxide radicals studied by optical spectroscopy. From left to right: NITCN, NITBzImH, NITPy.

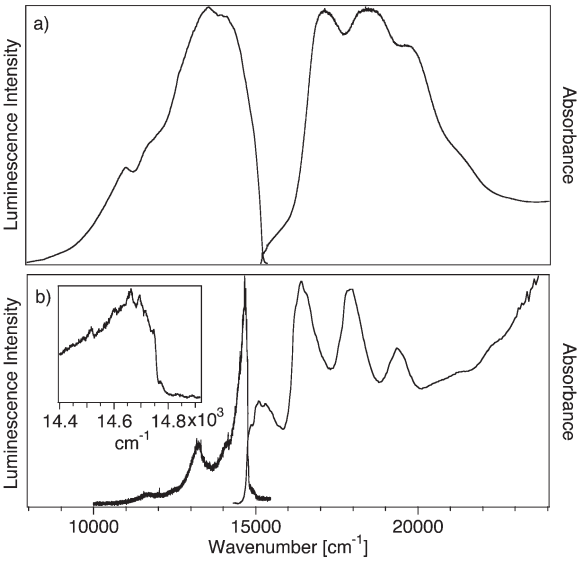

Fig. 2 Solid-state absorption and luminescence spectra of (a) NITPy and (b) NITBzImH measured at 5 K. The inset to (b) shows an enlarged view of the highest-energy luminescence transition of NITBzImH.

The luminescence intensities are low, indicating low quantum yields, and luminescence lifetimes are shorter than the lower limit of approximately 500 μs imposed by the near-infrared detector used. No luminescence was observed for the NITCN radical, likely due to efficient nonradiative relaxation processes involving the high-frequency C≡N vibrational mode or to efficient intermolecular energy transfer to killer traps in the solid. The luminescence spectrum of NITBzImH is well resolved and shows a short vibronic progression with an average interval of 1400 ± 30 cm^{-1}, as illustrated in Fig. 2b. Each member of this progression has a shoulder lower in energy by 650 ± 50 cm^{-1}, corresponding to at least one additional vibrational mode. The luminescence spectrum of NITPy also shows resolved maxima, but the resolution is not sufficient to clearly identify vibronic progressions. Nevertheless, two sets of maxima separated by 500 cm^{-1} are observed, an energy interval similar to that in the luminescence spectrum of NITBzImH. The energy separation between the two sets is on the order of 2300 cm^{-1}. All energy intervals determined from luminescence spectra are summarized in Table 1.

It is surprising that the luminescence spectra are not mirror images of the lowest-energy absorption bands. The absorption spectra in Figs. 2 and 3 have widths at half height estimated to be of the order of 4000 cm^{-1}, significantly larger than those of the luminescence bands in Fig. 2. Many nitronyl nitroxides and their transition metal complexes show absorption spectra with resolved patterns as illustrated in Figs. 2 and 3, consisting of a sequence of four to six peaks.[30,34] The energy differences between these maxima are constant within experimental precision between the high-energy peaks, but a different interval is observed between the lowest-energy transition, labeled band A in Figs. 3 and 4, and the next higher peak. This is well illustrated for NITBzImH, where band A is lower in energy by approximately 1200 cm^{-1} than the following band, but a larger difference of approximately 1500 cm^{-1} is observed between the maxima at higher energy. This latter interval is denoted by the progression labeled band B in Fig. 3. The energy intervals indicate that the sequence of peaks forming bands A and B in the absorption spectra does not correspond to a single vibronic progression, for which a constant energy separation is expected. This conclusion is confirmed by the intensity distribution within the band sequences in the luminescence and absorption spectra. The first member of the progression in

Table 1 Selected peak positions and energy intervals from absorption and luminescence spectra, Raman frequencies

Quantity	NITBzImH	NITPy	NITCN
Luminescence highest energy maximum/cm^{-1}	14 663	14 085	
Intervals/cm^{-1}	30	516	
	620	2334	
	1422	3072	
Absorption band A Lowest energy maximum/cm^{-1}	15 175	15 550	13 236
Intervals/cm^{-1}	208		310
Absorption band B Lowest energy maximum//cm^{-1}	16 367	17 199	14 892
Intervals/cm^{-1}	200	1270	364
	1523		462
			968
			1498
Raman frequencies/cm^{-1}	620		372
	778		523
	955		695
	1005		1263
	1135		1394
	1271		1444
	1365		1536
	1422		1604

the luminescence spectra has the highest intensity. The absorption spectrum should show the same intensity distribution if only a single excited state were involved. The experimental absorption spectra have a very different intensity distribution: the lowest energy peak is much less intense than the following higher energy bands. This is most obvious in the spectra of NITPy in Fig. 2a, where the intensity of the first peak is lower by at least an order of magnitude than that of the following bands. To the best of our knowledge, the results in Fig. 2 are the first comparison of full luminescence and absorption spectra for nitronyl nitroxides, and we will discuss the implications of the observed energy differences and intensity distributions in the following section.

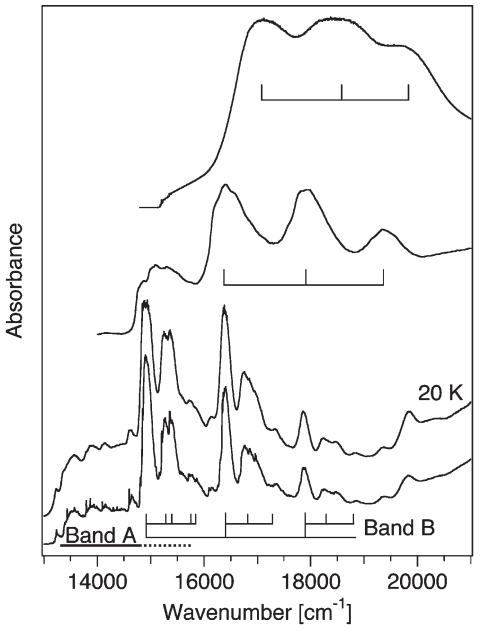

Fig. 3 Solid-state absorption spectra of NITPy, NITBzImH and NITCN (top to bottom). All spectra were measured at 5 K, except for one spectrum of NITCN, which was measured at 20 K, as indicated in the figure.

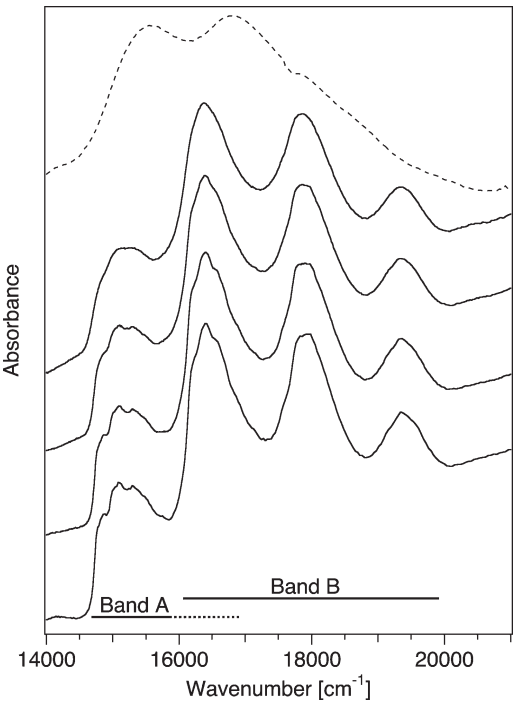

Fig. 4 Temperature dependent absorption spectra of NITBzImH. The top spectrum, shown as a dotted line, was measured at room temperature. Temperatures for the spectra shown as solid lines are 77 K, 40 K, 20 K and 5 K (top to bottom).

The detailed view of the highest-energy luminescence transition for NITBzImH in the inset to Fig. 2b shows resolved low-frequency vibronic structure in the luminescence spectrum. The average interval is on the order of 30 cm^{-1}, significantly less than the interval of 208 cm^{-1} in the lowest-energy absorption band for this compound. These small energy separations could be due to delocalized vibrational modes in the crystal. The intensity distribution within these energetically close resolved transitions is not identical in luminescence and absorption spectra and it has been shown that the patterns for uncoordinated free radicals and their lanthanide complexes are not identical.[30] These differences again underline that the lowest-energy electronic transitions provide very detailed spectroscopic information for the characterization of molecular materials based on nitronyl nitroxide radicals.

Fig. 3 shows the absorption spectra throughout the visible wavelength range for all three radicals illustrated in Fig. 1. All absorption band systems are similar and consist of a weak lowest-energy band, corresponding to the luminescence transition discussed above and denoted as band A in Fig. 3. The set of absorption spectra in Fig. 3 shows clearly that the weak, lowest-energy absorption bands are not the first member of the intense progressions at higher energy, in agreement with the conclusion based on the comparison of absorption and luminescence spectra in Fig. 2. The lowest-energy absorption band is the mirror image of the luminescence spectrum and its higher energy components are in the energy range given by the dotted line segment for band A in Fig. 3, masked by the more intense bands corresponding to a different electronic transition. This higher-energy band system is labeled as band B and shows resolved progressions with at least three members, the first of which is most intense. The progressions are indicated on the spectra by the grids in Fig. 3 and the progression intervals determined from the spectra are summarized in Table 1. The best resolution is observed for the NITCN radical, shown at the bottom of Fig. 3. Two spectroscopic features are specific to the NITCN radical. First, a series of very sharp

peaks at 5 K is observed for band A. These peaks are no longer observed at 20 K and they have been assigned as cooperative magnetic excitations.[13] Second, the higher energy band B shows vibronic structure involving at least three vibrational modes with frequencies of 1500 ± 20 cm^{-1}, 470 ± 20 cm^{-1} and 360 ± 20 cm^{-1}.

Fig. 4 shows the temperature dependence of the absorption spectrum of NITBzImH. The low-frequency vibronic features are well resolved at 5 K, but this resolution disappears even at 77 K. The intensity distribution of the low-frequency resolved bands in the lowest frequency peak, denoted as band A, is different from the following higher-energy peaks, denoted as band B. This difference again illustrates that two overlapping electronic transitions to different excited states are observed. The band maxima of the main vibronic progression shift by less than 15 cm^{-1} in this temperature range. The room temperature spectrum, shown as a dotted line in Fig. 4, has less resolution and the band maxima are shifted to lower energy by 380 cm^{-1} compared to their positions at 77 K. This shift can be due to both vibrational hot bands or slight structural changes with temperature that influence the energies of the electronic states. The integrated intensities of bands A and B are independent of temperature, indicating the absence of efficient vibronic intensity mechanisms.

Discussion

Assignment of low-energy excited states

The comparison of luminescence and absorption spectra in Figs. 2 and 3 shows that transitions to at least two excited states form the observed absorption band system. This experimental conclusion is based on both the luminescence band shape that is not a mirror image of the absorption band and on the different shapes of absorption bands A and B in Figs. 3 and 4. Electronic structure calculations leading to the molecular orbital energy level schemes illustrated in Fig. 5 and Table 2 further confirm the presence of several excitations in the range of the experimental absorption spectra. Density functional calculations[35] were carried out using the crystallographic structures[13,36,37] of the three radicals shown schematically in Fig. 1 in order to obtain the molecular orbitals. The unpaired electron occupies the SOMO orbital, located on the nitroxide group, as has been characterized in detail by both theoretical calculations and experimental measurements of the unpaired spin density.[4,38–40] For all three radicals studied here, qualitatively similar energy level schemes are obtained, as illustrated in Fig. 5: the energy differences ΔE_1 and ΔE_2 separating the SOMO from the SOMO − 1 and SOMO + 1 levels, respectively, are of comparable

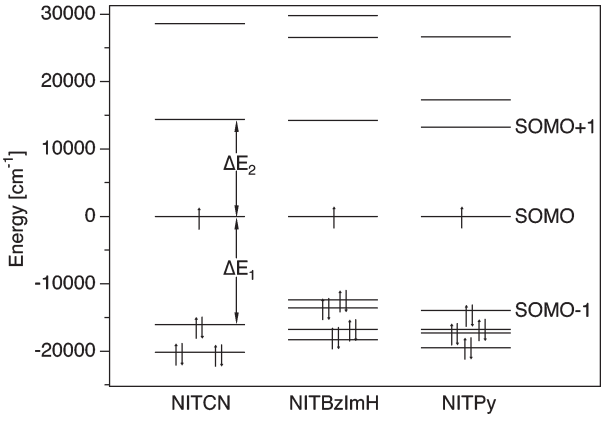

Fig. 5 Calculated molecular orbital energy levels of NITCN, NITBzImH and NITPy obtained with density-functional theory. The energies of the SOMO orbitals are set to 0 for this diagram.

Table 2 Calculated molecular orbital energies using density functional theory. Orbitals are identified by the same labels as in Fig. 5. The energy of the SOMO orbital was set to 0 for all three compounds and all energies are given in cm^{-1}

Orbital	NITCN	NITBzImH	NITPy
SOMO − 4	−33 544	−18 295	−19 471
SOMO − 3	−20 174	−16 753	−17 279
SOMO − 2	−20 172	−13 596	−16 789
SOMO − 1	−16 058	−12 396	−13 963
SOMO	0	0	0
SOMO + 1	14 389	14 222	13 219
SOMO + 2	28 592	26 522	17 244
SOMO + 3	35 284	29 796	26 631
SOMO + 4	42 160	34 034	33 371
SOMO + 5	45 931	39 399	39 634

magnitude. It can therefore be expected that excited electronic states arising from the $(SOMO - 1)^1(SOMO)^2$ and $(SOMO)^0(SOMO + 1)^1$ excited electron configurations are observed at similar energies and are expected to lead to overlapping absorption bands. The molecular orbitals in Fig. 6 can be used to estimate intensities for transitions between electronic states arising from different orbital configurations.[41] We compare the SOMO → SOMO + 1 and SOMO − 1 → SOMO excitations. The most important quantity to consider is the heuristic transition density, corresponding to the product of the two orbitals involved in the excitation.[41] We discuss this quantity in the same qualitative manner given for the HMO model in the literature.[41] If the overlap between orbitals of the initial and final configurations is small, the transition density is low, resulting in a weak band. In addition, for orbitals with significant overlap, the heuristic transition density can be low if there is no net charge redistribution, corresponding to the parity selection rule.[41] For NITCN, the product of the SOMO − 1 and SOMO orbitals is very small, as the former orbital has its main probability density in the plane of the molecule, the latter perpendicular to this plane. In addition, the sequence of black-to-grey color changes along the O–N–N–O fragment, the "phase" of the orbitals, are identical. The SOMO − 1 → SOMO excitation is therefore expected to lead to a weak band. In contrast, the SOMO and SOMO + 1 orbitals are

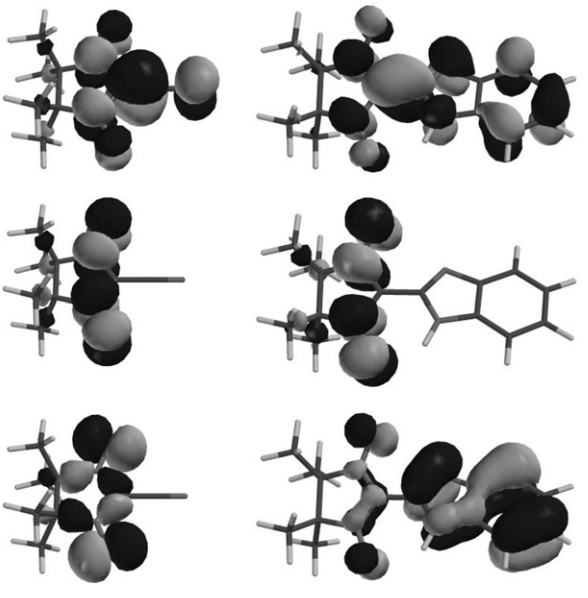

Fig. 6 Calculated molecular orbitals for NITCN (left-hand column) and NITBzImH (right-hand column). The SOMO + 1, SOMO and SOMO − 1 orbitals are shown from top to bottom.

both perpendicular to the plane of the molecule and their different phases lead to a large transition density and an intense electronic transition. This comparison shows that the molecular orbital calculations for NITCN correctly indicate that both weak and more intense low-energy electronic transitions can occur. The comparison of the same two excitations for NITBzImH shows that they both lead to nonzero transition densities based on their phases. The different intensities arise because of the amount of electron density that is delocalized onto the benzimidazole ring system. This density is estimated to be largest for the SOMO + 1 orbital, leading to a weaker band than for the SOMO − 1 → SOMO excitation. This qualitative analysis confirms therefore that one of the two lowest-energy absorption bands of NITBzImH is expected to be significantly weaker than the other. Calculated oscillator strengths for the two lowest-energy electronic transitions of NITBzImH using an advanced density functional method[42] and a computationally optimized molecular structure are 5×10^{-4} and 1×10^{-2} with calculated absorption maxima at 11 500 cm^{-1} and 12 700 cm^{-1}, respectively, lower by approximately 4000 cm^{-1} than the experimental band maxima in Fig. 4. These calculations therefore also suggest the presence of two electronic transitions separated by 1200 cm^{-1} for NITBzImH, in very good agreement with the energy difference derived from the spectra in Figs. 3 and 4. The calculated oscillator strengths confirm that the lowest-energy band is weak. The experimental oscillator strength determined from the solution absorption spectrum of NITBzImH in dichloromethane is 1.2×10^{-2} for bands A and B combined, similar to estimated oscillator strengths from solution spectra of other nitronyl nitroxides in the literature,[28] and in excellent agreement with the total oscillator strength of 1.05×10^{-2} obtained from the calculation. All density functional calculations therefore support the spectroscopic analysis concluding that the absorption band system observed between approximately 14 000 cm^{-1} and 21 000 cm^{-1} shown in Fig. 3 corresponds to two different electronic transitions.

Vibronic structure in absorption and luminescence spectra

The molecular orbital pictures can be used to qualitatively characterize the vibronic structure in the absorption and luminescence spectra shown in Figs. 2 to 4. The main change in electron density for the two lowest-energy excited configurations occurs on the nitroxide group, as illustrated by the orbitals for NITCN and NITBzImH in Fig. 6. As a consequence, the O–N–C–N–O bond lengths show the largest differences between the ground state and the low-energy excited states discussed here, and modes involving this fragment form the observed progressions. Experimental energy intervals and intensities determined from the vibronic structure of the luminescence and absorption spectra are used to quantitatively analyze the structural changes along normal coordinates between the ground and low-energy excited states.[43] An appealing spectrum for such an analysis is the resolved luminescence spectrum of NITBzImH in Fig. 2b. The intervals defining its vibronic structure correspond to vibrational frequencies observed in the Raman spectrum as summarized in Table 1. The spectrum can be calculated by assuming harmonic potential energy surfaces for both the ground and excited states.

The potential energy surface of the excited state is given by eqn (1):

$$E = \frac{1}{2}\sum_k \omega_k (Q_k - \Delta_k)^2 \qquad (1)$$

where k numbers the dimensionless normal coordinates Q_k with frequency ω_k. The minimum of the excited state potential energy surface is offset along each normal coordinate by Δ_k. These offsets are the only unknown quantities and will be determined from the calculations of absorption and luminescence spectra described in the following. For the calculation of the luminescence spectrum of NITBzImH we assume identical vibrational frequencies for the ground and emitting states. The luminescence intensity I as a function of the wavenumber ω is given by eqn. (2):[43–45]

$$I(\omega) = C\omega^x \int_{-\infty}^{\infty} e^{i\omega t} e^{\sum_k \left(-\frac{\Delta_k^2}{2}(1-e^{-i\omega_k t}) - \frac{i\omega_k t}{2}\right) - iE_{00}t - \Gamma^2 t^2} \mathrm{d}t \qquad (2)$$

In this equation, C is a scaling factor, x is equal to 3 for a luminescence transition, E_{00} denotes the energy of the electronic origin transition and Γ is a phenomenological damping factor defining the linewidth of each vibronic band in the calculated spectrum. Only normal coordinates Q_k with nonzero offsets Δ_k have to be considered for the calculation of the vibronic bandshape considered here. The energy of the electronic origin, E_{00}, always corresponds to the highest energy luminescence transition and, in the absence of vibronic origins, to the first member of the vibronic progressions. From the spectra in Fig. 2 and Fig. 3, E_{00} can be evaluated to within 100 cm^{-1}. The damping factor Γ is adjusted to give an acceptable overall calculated width for each vibronic band and a value of 80 cm^{-1} is obtained. Fig. 7a shows the comparison of experimental and calculated luminescence spectra of NITBzImH. The simple model calculation based on offsets along only two normal coordinates leads to a satisfactory agreement with the experimental spectrum. All resulting parameters are summarized in Table 3. Two experimental vibrational frequencies determined from the luminescence spectrum, 1422 cm^{-1} and 620 cm^{-1}, are sufficient to calculate the spectrum in Fig. 7a and they are close to the frequencies of 1325 cm^{-1}, 1432 cm^{-1}, 1455 cm^{-1} and

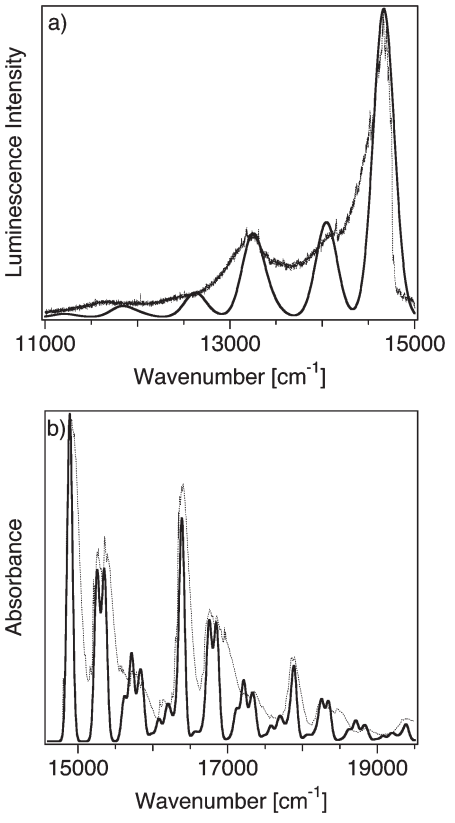

Fig. 7 Comparison of experimental and calculated spectra, shown as dotted and solid lines, respectively. (a) Luminescence of NITBzImH. (b) Absorption of NITCN, second-lowest energy transition (band B in Fig. 3).

Table 3 Parameter values used to calculate the luminescence and absorption spectra in Fig. 7

Parameter	NITBzImH Luminescence spectrum	NITCN Absorption spectrum
E_{00}/cm^{-1}	14 663	14 892
ω_k/cm^{-1}, Δ_k	1422, 0.84	1498, 1.52
	620, 0.84	982, 1.00
		470, 1.41
		360, 1.41
Γ/cm^{-1}	80	25

556 cm^{-1}, 578 cm^{-1}, 704 cm^{-1} resulting from electronic structure calculations[35] with normal coordinates involving the O–N–C–N–O fragment, as derived from the molecular orbital calculations in the preceding section.

The same approach can be applied to the absorption spectra.[43–45] We analyze the absorption spectrum of NITCN because it shows the best resolution of the three compounds, and calculate band B. The experimental spectrum shows several distinct energy differences and more than two vibrational modes form the resolved vibronic structure. Their frequencies are easily determined from the absorption spectrum in Fig. 3 because the individual vibronic bands are narrower than for the luminescence spectrum in Fig. 7a and a smaller damping factor Γ of 25 cm^{-1} is used for the calculation. The excited-state vibrational frequencies are not expected to be exactly identical to the ground-state transitions measured by Raman spectroscopy. The excited state potential energy surface is again given by eqn. (1) and the absorption spectrum can be calculated with eqn. (2), using a value of 1 for x. The resulting parameters are summarized in Table 3. The vibrational frequencies chosen for the calculation of the spectrum are again supported by the frequencies obtained from electronic structure calculations.[35] Three modes are calculated at 352 cm^{-1}, 361 cm^{-1} and 372 cm^{-1}, close to the experimental frequency of 360 cm^{-1} determined from the absorption spectrum. The calculated frequency of 613 cm^{-1} is close to the experimental interval of 470 cm^{-1}, and calculated frequencies of 884 cm^{-1}, 924 cm^{-1}, 970 cm^{-1}, and 993 cm^{-1} correspond to the experimental frequency of 982 cm^{-1}. Finally, calculated frequencies of 1454 cm^{-1} and 1557 cm^{-1} are close to the experimental interval of 1498 cm^{-1}. All of these modes involve the atoms with significant SOMO electron density, but due to the low symmetry and high number of atoms in all title compounds, it is not possible to provide intuitively appealing visualizations of the coordinates. We note that the molecular orbital calculation gives ground-state frequencies, but excited-state frequencies define the vibronic patterns in the calculated absorption spectrum in Fig. 7b. The calculated values provide therefore a reasonable approximation allowing the assignment of vibronic intervals in the absorption spectrum of NITCN in Fig. 3.

Larger offsets Δ_k are observed for NITCN than for NITBzImH. This can be rationalized qualitatively from Fig. 6, where the change in bonding between SOMO and SOMO + 1 is more pronounced for NITCN than for NITBzImH. The delocalization of electron density onto the aromatic ring system of NITBzImH dilutes these changes, leading to weaker bonding changes and smaller Δ_k values and also to its less resolved absorption spectrum. Nevertheless, the overall characteristics of these low-energy excited states are similar. The main structural difference between the ground state and the low-energy excited states involves the bonds in the region of high unpaired electron density. The analysis of our low-temperature absorption and luminescence spectra shows that nitronyl nitroxides have several excited states in the visible region of the optical spectrum. They can be characterized from their resolved vibronic structure.

Acknowledgements

We thank Professor Matthias Ernzerhof (Université de Montréal) for help with the density functional calculations. Financial support from the Natural Sciences and Engineering Research Council (Canada), the Centre Jacques Cartier and the Commission Permanente de Coopération Franco-Québécoise is gratefully acknowledged.

References

1 J. S. Miller and A. J. Epstein, *Molecule Based Magnet*, eds. J. S. Miller and A. J. Epstein, *MRS Bulletin*, Materials Research Society, Warrendale, PA, 2000, vol. 25, issue 11.
2 E. Coronado, J. R. Galan-Mascaros, C. J. Gomez-Garcia and V. Laukhin, *Nature*, 2000, **408**, 447.
3 O. Kahn, *Adv. Inorg. Chem.*, 1996, **43**, 179.
4 C. Benelli and D. Gatteschi, *Chem. Rev.*, 2002, **102**, 2369.
5 C. Mathonière, O. Kahn, J. C. Daran, H. Hilbig and F. H. Kohler, *Inorg. Chem.*, 1993, **32**, 4057.
6 C. Mathonière and O. Kahn, *Inorg. Chem.*, 1994, **33**, 2103.
7 P. J. McCarthy and H. U. Güdel, *Coord. Chem. Rev.*, 1988, **88**, 69.
8 P. M. Lahti, *Magnetic Properties of Organic Materials*, Marcel Dekker, Inc., New York, 1999.
9 M. Kinoshita, P. Turek, M. Tamura, K. Nozawa, D. Shiomi, Y. Nakazawa, M. Ishikawa, M. Takahashi, K. Awaga, T. Inabe and Y. Maruyama, *Chem. Lett.*, 1991, 1225.
10 J. Cirujeda, M. Mas, E. Molins, F. Lanfranc de Panthou, J. Laugier, J. G. Park, C. Paulsen, P. Rey, C. Rovira and J. Veciana, *J. Chem. Soc., Chem. Commun.*, 1995, 709.
11 A. Caneschi, F. Ferraro, D. Gatteschi, A. Le Lirzin, M. A. Novak, E. Rentschler and R. Sessoli, *Adv. Mater.*, 1995, **7**, 476.
12 F. M. Romero, R. Ziessel, M. Drillon, J. L. Tholence, C. Paulsen, N. Kyritsakas and J. Fisher, *Adv. Mater.*, 1996, **8**, 826.
13 C. Hirel, D. Luneau, J. Pécaut, L. Öhrström, G. Bussière and C. Reber, *Chem. Eur. J.*, 2002, **8**, 3157.
14 K. Inoue and H. Iwamura, *J. Am. Chem. Soc.*, 1994, **116**, 3173.
15 K. Inoue, T. Hayamizu, H. Iwamura, D. Hashizume and Y. Ohashi, *J. Am. Chem. Soc.*, 1996, **118**, 1803.
16 H. Iwamura, K. Inoue and N. Koga, *New. J. Chem.*, 1998, 201.
17 C. Lescop, D. Luneau and P. Rey, *Mater. Res. Soc. Symp. Proc.*, 2000, **598**, BB3.49.1.
18 K. Fegy, D. Luneau, T. Ohm, C. Paulsen and P. Rey, *Angew. Chem., Int. Ed.*, 1998, **37**, 1270.
19 A. Caneschi, D. Gatteschi, R. Sessoli and P. Rey, *Acc. Chem. Res.*, 1989, **22**, 392.
20 K. Matsuda and M. Irie, *J. Am. Chem. Soc.*, 2000, **122**, 7195.
21 M. Nakano, S. Yamada and K. Yamagushi, *Bull. Chem. Soc. Jpn.*, 1998, **71**, 845.
22 E. F. Ullman, J. H. Osiecki, D. G. B. Boocock and R. Darcy, *J. Am. Chem. Soc.*, 1972, **94**, 7049.
23 N. M. Karayannis, C. M. Paleos, C. M. Mikulski, L. L. Pytlewski, H. Blum and M. M. Labes, *Inorg. Chim. Acta*, 1973, **7**, 74.
24 P. F. Richardson and R. W. Kreilick, *J. Am. Chem. Soc.*, 1977, **99**, 8183.
25 T. Yoshida, K. Kanamori, S. Takamizawa, W. Mori and S. Kaizaki, *Chem. Lett.*, 1997, 603.
26 T. Yoshida, T. Suzuki, K. Kanamori and S. Kaizaki, *Inorg. Chem.*, 1999, **38**, 1059.
27 T. Tsukuda, T. Suzuki and S. Kaizaki, *J. Chem. Soc., Dalton Trans.*, 2002, 1721.
28 M. Ogita, Y. Yamamoto, T. Suzuki and S. Kaizaki, *Eur. J. Inorg. Chem.*, 2002, 886.
29 Y. Tsukahara, A. Iino, T. Yoshida, T. Suzuki and S. Kaizaki, *J. Chem. Soc., Dalton Trans.*, 2002, 181.
30 C. Lescop, D. Luneau, G. Bussière, M. Triest and C. Reber, *Inorg. Chem.*, 2000, **39**, 3740.
31 C. Lescop, E. Belorizky, D. Luneau and P. Rey, *Inorg. Chem.*, 2002, **42**, 3375.
32 M. J. Davis and C. Reber, *Inorg. Chem.*, 1995, **34**, 4585.
33 G. Bussière, R. Beaulac, B. Cardinal-David and C. Reber, *Coord. Chem. Rev.*, 2001, **219–221**, 509.
34 C. Lescop, D. Luneau, P. Rey, G. Bussière and C. Reber, *Inorg. Chem.*, 2002, **41**, 5566.
35 MacSpartan Pro, version 1.0.4, Wavefunction Inc., Irvine, CA 92612, 2000. Molecular orbitals were calculated with the SVWN density functional method and DN* basis set. Vibrational frequencies were calculated with the PM3 method.

36 V. Barone, A. Grand, D. Luneau, P. Rey, C. Minichino and R. Subra, *New J. Chem.*, 1993, **17**, 545.
37 N. Yoshioka, M. Irasawa, Y. Mochizuki, T. Kato, H. Inoue and S. Ohba, *Chem. Lett.*, 1997, 251.
38 A. Zheludev, V. Barone, M. Bonnet, B. Delley, A. Grand, E. Ressouche, P. Rey, R. Subra and J. Schweizer, *J. Am. Chem. Soc.*, 1994, **116**, 2019.
39 A. Zheludev, M. Bonnet, D. Luneau, E. Ressouche, P. Rey and J. Schweizer, *Physica B: (Amsterdam)*, 1995, **213&214**, 268.
40 E. Ressouche, J. X. Boucherle, B. Gillon, P. Rey and J. Schweizer, *J. Am. Chem. Soc.*, 1993, **115**, 3610.
41 E. Heilbronner and H. Bock, *Das HMO Modell und seine Anwendung*, Verlag Chemie, Weinheim, 1968, vol. I, p. 303.
42 Gaussian-99, M. J. Frisch, G. W. Trucks, H. B. Schlegel, G. E. Scuseria, M. A. Robb, J. R. Cheeseman, V. G. Zakrzewski, J. A. Montgomery Jr, R. E. Stratmann, J. C. Burant, S. Dapprich, J. M. Millam, A. D. Daniels, K. N. Kudin, M. C. Strain, O. Farkas, J. Tomasi, V. Barone, B. Mennucci, M. Cossi, C. Adamo, J. Jaramillo, R. Cammi, C. Pomelli, J. Ochterski, G. A. Petersson, P. Y. Ayala, K. Morokuma, D. K. Malick, A. D. Rabuck, K. Raghavachari, J. B. Foresman, J. V. Ortiz, Q. Cui, A. G. Baboul, S. Clifford, J. Cioslowski, B. B. Stefanov, G. Liu, A. Liashenko, P. Piskorz, I. Komaromi, R. Gomperts, R. L. Martin, D. J. Fox, T. Keith, M. A. Al-Laham, C. Y. Peng, A. Nanayakkara, M. Challacombe, P. M. W. Gill, B. Johnson, W. Chen, M. W. Wong, J. L. Andres, C. Gonzalez, M. Head-Gordon, E. S. Replogle and J. A. Pople, Gaussian Inc., Pittsburgh PA, 2001.
43 J. I. Zink, *Coord. Chem. Rev.*, 2001, **211**, 69.
44 J. I. Zink and K.-S. K. Shin, *Adv. Photochem.*, 1991, **16**, 119.
45 E. J. Heller, *Acc. Chem. Res.*, 1981, **14**, 368.